Hindawi
International Journal of Aerospace Engineering
Volume 2020, Article ID 5754205, 14 pages
https://doi.org/10.1155/2020/5754205

Research Article

Center-of-Gravity Variation-Driven Spherical UAV System and Its Control Law

Donghoon Kim and Sungwook Yang

University of Cincinnati, Cincinnati, OH 45221, USA

Correspondence should be addressed to Donghoon Kim; donghoon38.kim@gmail.com

Received 20 November 2019; Revised 25 January 2020; Accepted 14 February 2020; Published 7 April 2020

Guest Editor: Zongyu Zuo

Most of the spherical unmanned aerial vehicles (SUAVs) use control surfaces, which are functions of aileron and an elevator, to generate control torque. The work proposes a new conceptual design of an SUAV system controlled through center-of-gravity (CG) variations with its path-tracking control law designed for the system. Compared to the one using control surfaces, the concept suggested is beneficial in the aspect of the expandability of building lighter and smaller SUAVs, especially. A CG variation principle by actuating a pendulum type of a moving part is considered as a methodology for both translational and rotational motion control of an SUAV. Since variations of the moment-of-inertia (MOI) elements which resulted from the motion of the moving part affect the performance of the suggested method, the variations of MOI analysis are performed for all angular ranges of the moving part. As a result, certain angular ranges for the moving part to prevent the degradation of the path-tracking performance by the effect of the MOI changes are found. By considering the findings, numerical studies are performed for hovering, ascent, descent, and horizontal tracking missions. The applicability of the proposed SUAV system and the corresponding controller to achieve the path-tracking missions is demonstrated through the numerical simulation.

1. Introduction

Researches for the various shapes of unmanned aerial vehicles (UAVs) have been performed continuously because of the variety of UAVs' application areas: reconnaissance, delivery, rescue, monitoring, etc. [1–4]. Among the several types of UAVs, spherical UAVs (SUAVs) do not require using multiple rotors. In this regard, the SUAVs have various advantages in terms of compactness, lightness, inexpensiveness, etc. [1].

Malandrakis et al. and Loh and Jacob demonstrated SUAVs consist of a contrarotating (parts of a mechanism rotate in opposite directions about a common axis) motor and several control vanes [5, 6]. The contrarotating motor is used to minimize the reaction torque generated by the motor rotation, and a classical proportional-integral-derivative (PID) control law is applied for attitude control. Position control is not considered for these two SUAVs. In Ref. [6], an ultrasonic sensor is applied for altitude control. Sato Humiyuki and Technical Research and Development Institute of Japan's Ministry of Defense developed an SUAV called Japan Flying Sphere where the propulsion system consists of a single motor and eight control vanes [7]. Kim et al. developed a rotary-wing micro aerial vehicle that has the same concept of operations as an SUAV using a single motor, four antitorque vanes, and three control vanes [8]. In these aerial vehicles, control vanes play a role as an aileron, an elevator, and a rudder of fixed-wing aerial vehicles to generate torque for attitude control. As one of the techniques for generating the control torque, the moving center-of-gravity (CG) was studied and considered in attitude and position controls. Bouabdallah et al. and Bermes et al. suggested a CG shifting system, which is designed to control horizontal motions, for an indoor coaxial helicopter [9, 10]. This research proposed a conventional independent proportional-derivative (PD) controller for attitude control. In Refs. [9, 10], a compensation method is introduced for altitude control using attitude angles and a distance measured by an infrared sensor. Seisan designed a coaxial helicopter including the moving mass system [11]. In Ref. [11], a nonlinear control law and a PD

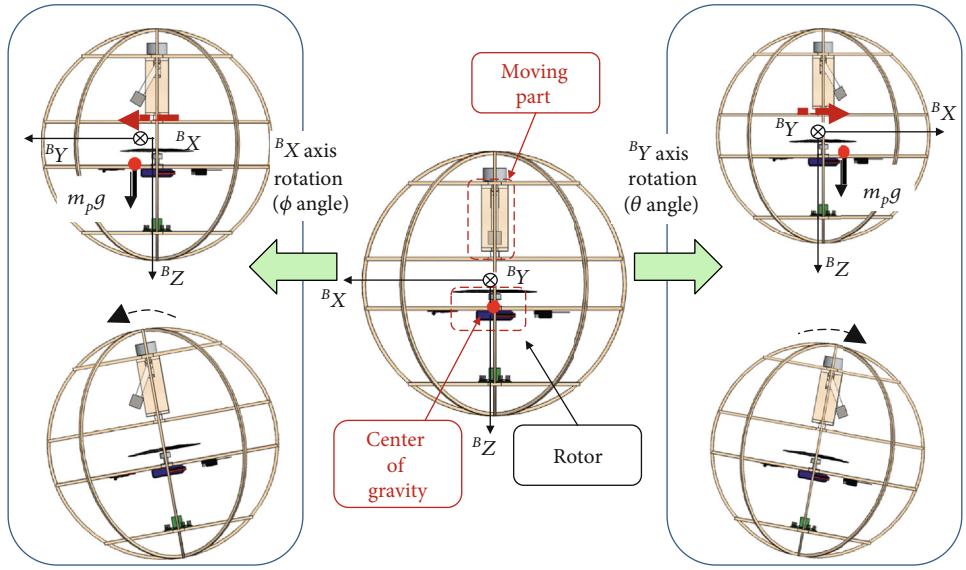

Figure 1: Operation concept using the suggested method.

control law are applied to manipulate position and attitude, respectively. All these SUAVs have vanes to control their attitude. These vanes are usually designed according to how much aerodynamic forces generate torques to control attitudes. Since these forces depend on the size of vanes, the size of the SUAV might be determined by the size of the vane. The main idea of our approach is to develop a smaller platform than a former SUAV by diminishing the size of the vane in the SUAV as possible.

The main objective of this paper is to show the feasibility of the proposed conceptual design for the SUAV and its operation. To do so, a control method for the SUAV is suggested by combining a CG variation technique, which generates appropriate torques, and a path-tracking controller. Equations of motion of the SUAV are derived, and the variations of CG are calculated by using control inputs. The applicability of the suggested method is affected by the varying moment-of-inertia (MOI) components, which vary with position and mass of the moving part. To generate more torques for large-angle maneuvers, a mass of the moving part or distance between a pivot point and the moving part must be increased. Varying these two factors, however, results in the variation of MOI components, which is not negligible. The analyses of MOI variations are conducted to see how MOI components are varied with respect to two factors. To avoid the large variation of MOI, two factors are constrained for generating small amount of torque, which leads to small-angle maneuvers. The applicability of the suggested methodology is validated through numerical simulation studies.

2. A Spherical UAV Control Technique

2.1. A Center-of-Gravity Variation Technique. An SUAV can be controlled by manipulating a thrust force and CG variations [12]. For a hovering purpose, both constant thrust force and torque are applied to maintain the position and attitude. A thrust force is only applied for vertical (altitude) movements. A translational motion along the X (north) and Y (east) axes in the inertial coordinate is related to θ and ϕ, respectively [13, 14]. The movement along the Z (down) axis in the inertial coordinate with respect to the altitude is controlled by the thrust force from a rotor. An attitude controller of the SUAV is able to attain a desired position on the X and Y axes, since the movements along the X and Y axes are accompanied by controlling θ and ϕ. The combination of the frame area of the SUAV and the reaction torque produced by the motor speed is used for ψ control [5]. The key in this work is the control of θ and ϕ using the torque generated by varying the CG. For rotating θ (or ϕ) with respect to a translation along the X (or Y) axis, the CG is moved along the X (or Y) axis, and u_θ (or u_ϕ) can be generated from a thrust force on the Z axis and the weight of a moving part in the SUAV. As the implementation strategy of the proposed method, one considers using a moving part, which is composed of motors and a pendulum, to change the CG of the SUAV. The position of the moving part can be manipulated by two motors: one is equipped on the top of the moving part, and the other is equipped on the frame of the moving part (see Figure 1). The upper and lower motors are in charge of manipulating the elevation angle α and the azimuth angle β, respectively. Since the space on the top of the SUAV is small to put in a sensor for measuring β, a stepping motor with a driver is considered as the upper motor, and this motor has a role in the control of β. The motor for controlling α is fitted on the rod that is connected to the motor for controlling β. There is enough space in order that a motor with a sensor for measuring α is equipped. Therefore, a DC motor with an encoder or a potentiometer could be an option for α control. When operating the moving part, in the case of varying attitude, the sequence of the control for the moving part is to rotate β and then α. On the other hand, attitude control for the SUAV uses the reverse sequence of

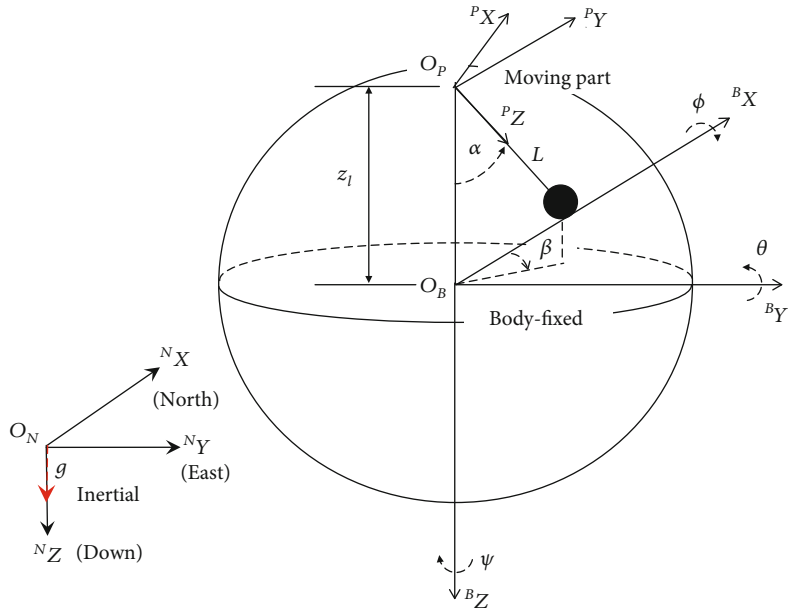

Figure 2: Configuration of the SUAV.

the moving part control. This is to prevent a reaction torque generated by the moving part in a case where α is not zero. Figure 1 describes an operation concept for the suggested control method.

For ψ control, u_ψ is generated by using the combination of the frame area of the SUAV and the main rotor speed. To rotate ψ, it is necessary to increase or decrease the rotor speed. The frame area creates the drag force, and this force generates the moment to prevent the reaction torque. Basically, the design of the frame area is based on the condition of the hovering status. Therefore, when increasing the rotor speed, the reaction torque is greater than the moment generated by the drag force and vice versa. Furthermore, the frame width generates a drag with respect to an angular velocity of a rotor in order that a moment of Z axis created by this method could curtail a reaction torque. The moment for a reduction of a reaction torque can be expressed as

$$M_z = \frac{1}{2} C_d h w l^3 \omega_z^2, \tag{1}$$

where M_z is the moment generated by the drag, C_d is the drag coefficient of a plate, h is the frame height, w is the frame width, l is the distance between the rotor and the center of the frame, and ω_z is the angular velocity of the Z axis in the body-fixed frame, respectively.

2.2. Calculation of Moment-of-Inertia Variation. Since the CG variation technique results in varying the mass properties, especially inertia properties, the dynamics of the SUAV has the parametric uncertainty caused by the proposed method. In other words, the angle of the moving part varies the inertia properties of the SUAV so the characteristic of the rotation dynamics is also changed by the varying inertia properties. Thus, the analysis of how much the inertia properties are varied by the movement of a moving part is necessary to determine system parameters which reduce the effect of the parametric uncertainty. Figure 2 describes a configuration of the SUAV including a moving part for varying the CG and coordinates to derive equations of motion for the SUAV. The angles α and β for a moving part can be controlled by two motors, and the operational angular ranges are as follows: (i) β operates all angular ranges and (ii) the angular operation range for α is limited to $|\alpha| \leq 90^\circ$ because of the rod length L and the pivot position of the moving part z_l. The rotations of α and β result in the variations of the CG, which generate torques for attitude control of the SUAV. For simplification in the formulation development, the body-fixed coordinate expression $^{B}(\cdot)$ and body description $(\cdot)_b$ for any variable are expressed by omitting the superscript B and the subscript b. Relatively much smaller product-of-inertia elements, which are negligible, are assumed. Then, the MOI elements of the body in the body-fixed coordinate are calculated by

$$J_k = J_{s,k} + J_{p,k} + m_p r_k^2, \tag{2}$$

where m is the mass, the subscript s denotes the sphere structure except a moving part, the subscript p denotes the moving part, and r_k is the perpendicular distance between the moving part and each axis ($k = x$, y, and z) in the body-fixed coordinate. It means that r_x is the distance between the X axis of rotation ϕ and the position of the moving part on the XY surface in the body-fixed coordinate and r_y and r_z can also be calculated in the same manner.

The relationship between the body-fixed and the moving part coordinates can be expressed by the direction cosine

matrix C_P^B, which transforms from P (moving part) to B (body-fixed) frame given the β-α transformation, as follows:

$$C_P^B = \begin{bmatrix} c\alpha c\beta & -s\beta & s\alpha c\beta \\ c\alpha s\beta & c\beta & s\alpha s\beta \\ -s\alpha & 0 & c\alpha \end{bmatrix}, \tag{3}$$

and $\mathbf{r}_\mathrm{p}$ is expressed in the body-fixed coordinate as

$$\mathbf{r}_\mathrm{p} \equiv \begin{bmatrix} r_{\mathrm{p},x} \\ r_{\mathrm{p},y} \\ r_{\mathrm{p},z} \end{bmatrix} = C_P^B {}^P\mathbf{r}_\mathrm{p} + \mathbf{o}_\mathrm{p} = \begin{bmatrix} Ls\alpha c\beta \\ Ls\alpha s\beta \\ Lc\alpha - z_l \end{bmatrix}, \tag{4}$$

where ${}^P\mathbf{r}_\mathrm{p} = [0, 0, L]^\mathrm{T}$, $\mathbf{o}_\mathrm{p} = [0, 0, -z_l]^\mathrm{T}$, and s and c are the sine and cosine functions, respectively. Using equation (4), r_k is calculated as

$$r_k = \begin{cases} r_x = \sqrt{r_{\mathrm{p},y}^2 + r_{\mathrm{p},z}^2} = \sqrt{L^2 s^2\alpha s^2\beta + (Lc\alpha - z_l)^2}, \\ r_y = \sqrt{r_{\mathrm{p},z}^2 + r_{\mathrm{p},x}^2} = \sqrt{L^2 s^2\alpha c^2\beta + (Lc\alpha - z_l)^2}, \\ r_z = \sqrt{r_{\mathrm{p},x}^2 + r_{\mathrm{p},y}^2} = Ls\alpha, \end{cases} \tag{5}$$

and substituting equation (5) into equation (2) yields

$$J_k = \begin{cases} J_x = J_{\mathrm{s},x} + J_{\mathrm{p},x} + m_\mathrm{p}\left(L^2 s^2\alpha s^2\beta + (Lc\alpha - z_l)^2\right), \\ J_y = J_{\mathrm{s},y} + J_{\mathrm{p},y} + m_\mathrm{p}\left(L^2 s^2\alpha c^2\beta + (Lc\alpha - z_l)^2\right), \\ J_z = J_{\mathrm{s},z} + J_{\mathrm{p},z} + m_\mathrm{p} L^2 s^2\alpha. \end{cases} \tag{6}$$

The variation of MOI elements with respect to α and β is defined as

$$\Delta J_k = \begin{cases} \Delta J_x = J_x - J_{x,\mathrm{idle}} = m_\mathrm{p} L(1 - c\alpha)\left(2z_l - L(1 + c\alpha)c^2\beta\right), \\ \Delta J_y = J_y - J_{y,\mathrm{idle}} = m_\mathrm{p} L(1 - c\alpha)\left(2z_l - L(1 + c\alpha)s^2\beta\right), \\ \Delta J_z = J_z - J_{z,\mathrm{idle}} = m_\mathrm{p} L^2 s^2\alpha = m_\mathrm{p} L^2\left(1 - c^2\alpha\right), \end{cases} \tag{7}$$

where the MOI elements at the idle position denote the static condition, and they are calculated at $\alpha = \beta = 0$. From equation (7), ΔJ_x, ΔJ_y, and ΔJ_z are close to zero for small α, but the effect of the variation of MOI elements must be considered when the angular operation range of α is larger.

From equation (7), the variation of MOI elements is the function of variables m_p, L, z_l, α, and β. The variables m_p, α, and β can be determined from the structure design of the SUAV while L and z_l are determined by considering the variation of MOI elements.

In equation (7), ΔJ_x and ΔJ_y have the maximum value of $2m_\mathrm{p} L z_l$ at $|\alpha| \le 90^\circ$ and $\forall\beta$. In the case of ΔJ_z, the maximum value is found as $m_\mathrm{p} L^2$ at the same condition of both α and β. The difference between the maximum values of ΔJ_x and ΔJ_z can be calculated as follows:

$$(\Delta J_x)_{\max} - (\Delta J_z)_{\max} = m_\mathrm{p} L(2z_l - L). \tag{8}$$

Since $2z_l - L$ in equation (8) is greater than zero according to $z_l \ge L$ from the configuration of the SUAV, the maximum value of ΔJ_z does not exceed the maximum value of both ΔJ_x and ΔJ_y.

By defining a variable $h = z_l/L$, ΔJ_x in equation (7) can be expressed as

$$\Delta J_x = \frac{m_\mathrm{p} z_l^2}{h^2}(1 - c\alpha)\left(2h - (1 + c\alpha)c^2\beta\right), \tag{9}$$

and the first and second derivatives of equation (9) with respect to h are found as

$$\begin{aligned} \frac{\partial \Delta J_x}{\partial h} &= \frac{2m_\mathrm{p} z_l^2}{h^2}(1 - c\alpha)\left(\frac{c^2\beta}{h}(1 + c\alpha) - 1\right), \\ \frac{\partial^2 \Delta J_x}{\partial h^2} &= \frac{2m_\mathrm{p} z_l^2}{h^3}(1 - c\alpha)\left(2 - \frac{3c^2\beta}{h}(1 + c\alpha) - 1\right). \end{aligned} \tag{10}$$

The maximum value of ΔJ_x can be found at $\partial \Delta J_x/\partial h = 0$ satisfying $\partial^2 \Delta J_x/\partial h^2 < 0$ from equation (10) except the case when $c\alpha$ equals to 1, which results in $\Delta J_x = 0$ as well. That is, h is found as

$$h = \frac{z_l}{L} = (1 + c\alpha)c^2\beta, \tag{11}$$

and the range of L with respect to z_l can be obtained as

$$\frac{z_l}{2} \le L \le z_l \le R, \tag{12}$$

where $0 \le c^2\beta \le 1$ at $\forall\beta$ and $1 \le 1 + c\alpha \le 2$ at $|\alpha| \le 90^\circ$. Equation (12) can be also derived by using ΔJ_y in the same manner.

Substituting equation (11) into equation (9) yields

$$\Delta J_x = m_\mathrm{p} z_l^2 t^2\left(\frac{\alpha}{2}\right)\frac{1}{c^2\beta}, \tag{13}$$

where t denotes the tangent function. The range of ΔJ_x can be expressed as

$$0 \le \Delta J_x \le m_\mathrm{p} z_l^2, \tag{14}$$

where $0 \le t^2(\alpha/2) \le 1$ at $|\alpha| \le 90^\circ$. Therefore, m_p and z_l can be calculated by using the maximum value of $\Delta J_x = m_\mathrm{p} z_l^2$ and vice versa. *Note that the maximum value of ΔJ_x, which is*

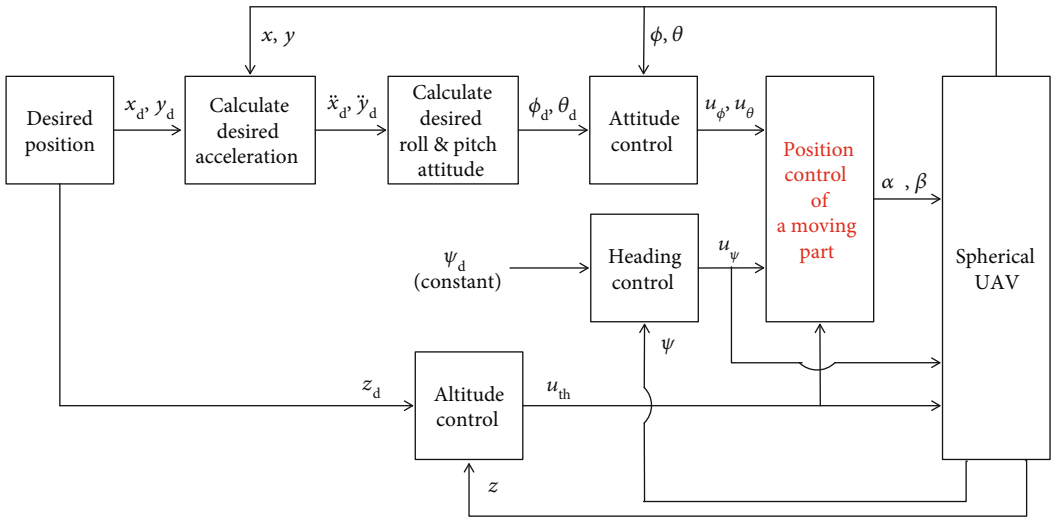

Figure 3: Control structure for the CG variation control scheme.

negligibly small, is determined by design parameters of the SUAV to avoid the large variation of MOI.

2.3. Path-Tracking Controller Design. Mathematical models for a rigid SUAV with respect to the attitude and the position in the body-fixed coordinate are generally expressed as [15]

$$M\dot{\mathbf{V}} + \boldsymbol{\omega} \times M\mathbf{V} = \mathbf{T}, \tag{15}$$

$$J\dot{\boldsymbol{\omega}} + \boldsymbol{\omega} \times J\boldsymbol{\omega} + \dot{J}\boldsymbol{\omega} = \boldsymbol{\tau}, \tag{16}$$

where $M \equiv \text{diag}\,(m, m, m)$, $J \equiv \text{diag}\,(J_x, J_y, J_z)$, $\mathbf{V} \in \mathscr{R}^3$ is the velocity, $\boldsymbol{\omega} \in \mathscr{R}^3$ is the angular velocity, $\mathbf{T} \in \mathscr{R}^3$ is the thrust, and $\boldsymbol{\tau} \in \mathscr{R}^3$ is the torque. As shown in Figure 2, α and β are required to control the SUAV, and the attitude angles are calculated by using control inputs. Note that the following assumptions are applied to design a path-tracking controller for the SUAV [13]: (i) in equation (15) $\mathbf{T} \gg \boldsymbol{\omega} \times M\mathbf{V}$; (ii) in equation (16) $\boldsymbol{\tau} \gg \boldsymbol{\omega} \times J\boldsymbol{\omega}$; (iii) in equation (16), $\dot{J}\boldsymbol{\omega}$ is relatively smaller than other terms; and (iv) ϕ and θ are relatively small. Because the propulsion system of the SUAV consists of one rotor and one propeller only, the thrust force for the SUAV is much smaller than the one for a UAV (e.g., a quadcopter) with the number of both motors and propellers. The low thrust force limits the total weight for the SUAV, and this leads to the mass budget limitation for a moving part. Thus, the SUAV only can generate a small amount of torque by controlling the moving part, and this limits the agile movement level. Also, the relatively lower speed of the SUAV helps to eliminate the effect of inertia component variation.

Applying (i), (ii), and (iii) into equations (15) and (16), leads to

$$\begin{aligned} {}^{N}\dot{\mathbf{V}} &= C_B^N M^{-1}\mathbf{T} + \mathbf{g}, \\ \ddot{\boldsymbol{\zeta}} &= J^{-1}\boldsymbol{\tau}, \end{aligned} \tag{17}$$

where $\mathbf{g} = [0, 0, g]^{\mathrm{T}}$, g is the gravity acceleration, $\boldsymbol{\zeta} = [\varphi, \theta, \psi]^{\mathrm{T}}$, $\mathbf{T} = [0, 0, u_{\mathrm{th}}]^{\mathrm{T}}$, and $\boldsymbol{\tau} = [u_\phi, u_\theta, u_\psi]^{\mathrm{T}}$. The matrix C_B^N, which transforms from B to N frame given the Euler 3-2-1 (ψ-θ-ϕ) transformation, is introduced as [16]

$$C_B^N = \begin{bmatrix} c\theta c\psi & s\phi s\theta c\psi - c\phi s\psi & c\phi s\theta c\psi + s\theta s\psi \\ c\theta s\psi & s\phi s\theta c\psi + c\phi c\psi & c\phi s\theta s\psi - s\phi c\psi \\ -s\theta & -s\phi c\theta & c\phi c\theta \end{bmatrix}, \tag{18}$$

where the superscript N denotes the inertial frame. Applying (iv) into equation (17), leads to

$$\begin{aligned} {}^{N}\ddot{x} &= (\theta c\psi + \phi s\psi)\frac{u_{\mathrm{th}}}{m}, \\ {}^{N}\ddot{y} &= (\theta s\psi - \phi c\psi)\frac{u_{\mathrm{th}}}{m}, \end{aligned} \tag{19}$$

$${}^{N}\ddot{z} = g + \frac{u_{\mathrm{th}}}{m}, \tag{20}$$

$$\begin{aligned} \ddot{\phi} &= \frac{u_\phi}{J_x}, \\ \ddot{\theta} &= \frac{u_\theta}{J_y}, \\ \ddot{\psi} &= \frac{u_\psi}{J_z}, \end{aligned} \tag{21}$$

where u is the control command, and the subscript th denotes the thrust.

The desired acceleration $\mathbf{a}_{\mathrm{d}} = [\ddot{x}_{\mathrm{d}}, \ddot{y}_{\mathrm{d}}, \ddot{z}_{\mathrm{d}}]^{\mathrm{T}}$ for the path-tracking task is generated from the classical PID control laws given as

$${}^{N}\mathbf{a}_{\mathrm{d}} = K_a\mathbf{e} + D_a\dot{\mathbf{e}} + I_a\int \mathbf{e}dt, \tag{22}$$

where the subscript d denotes the desired state, $\mathbf{e} \in \mathscr{R}^3$ is the position error in the inertial coordinate with respect to the

Table 1: Desired trajectory.

Index	Time (sec)	Target position (m)	Phase
—	0	(0, 0, 0)	Initial position
A	$0 < t \leq 10$	(0, 0, -10)	Ascent
B	$10 < t \leq 15$	(0, 0, -10)	Hovering
C	$15 < t \leq 25$	(10, 10, -10)	Horizontal movement
D	$25 < t \leq 30$	(10, 10, -10)	Hovering
E	$30 < t \leq 40$	(20, 0, -20)	Ascent and horizontal movement
F	$40 < t \leq 45$	(20, 0, -20)	Hovering
G	$45 < t \leq 55$	(10, -10, -10)	Descent and horizontal movement
H	$55 < t \leq 60$	(10, -10, -10)	Hovering
I	$60 < t \leq 70$	(0, 0, -10)	Horizontal movement
J	$70 < t \leq 80$	(0, 0, 0)	Descent

Table 2: Simulation parameters.

Parameter	Symbol	Value
Simulation time (sec)	t	80
Time interval (sec)	Δt	0.10
Total mass (kg)	m	0.51
Moving part mass (kg)	m_{p}	0.01
Radius of the SUAV (m)	R	0.25
Pivot position of the moving part (m)	z_l	0.25
Rod length (m)	L	0.125
Inertia components ($\mathrm{kg} \cdot \mathrm{m}^2$)	J_x	126.57×10^{-5}
	J_y	126.57×10^{-5}
	J_z	125.02×10^{-5}
Scalar gains for control	k_a	1.9608
	d_a	1.5686
	i_a	0.0980
	k_τ	6.2000
	d_τ	2.2000

desired path. The gain matrices are defined as mass functions as follows: $K_a = k_a M$, $D_a = d_a M$, and $I_a = i_a M$, where k_a, d_a, and i_a are scalars.

From equations (20) and (22), u_{th} is expressed as

$$u_{\mathrm{th}} = m^2 \left(k_a e_z + d_a \dot{e}_z + i_a \int e_z \mathrm{d}t - \frac{g}{m} \right). \tag{23}$$

The rapid manipulation of the moving part leads to the drastic attitude change for the SUAV, and this generates the overshoot of the system response. To generate the faster-damped response for the system, PD control law rather than PID control law that shows lesser damping is considered for the SUAV attitude control. Thus, the control input is defined as

$$\boldsymbol{\tau} = K_{\boldsymbol{\tau}}(\boldsymbol{\zeta}_{\mathrm{d}} - \boldsymbol{\zeta}) + D_{\boldsymbol{\tau}}\left(\dot{\boldsymbol{\zeta}}_{\mathrm{d}} - \dot{\boldsymbol{\zeta}}\right), \tag{24}$$

and the gain matrices are defined as MOI functions as follows: $K_\tau = k_\tau J$ and $D_\tau = d_\tau J$, where k_τ and d_τ are scalars. Substituting ϕ_{d}, θ_{d}, and ψ_{d} into equations (19) and (22) yields [17]

$$\begin{bmatrix} \phi_{\mathrm{d}} \\ \theta_{\mathrm{d}} \end{bmatrix} = \frac{m}{u_{\mathrm{th}}} \begin{bmatrix} \mathrm{s}\psi_{\mathrm{d}} & -\mathrm{c}\psi_{\mathrm{d}} \\ \mathrm{c}\psi_{\mathrm{d}} & \mathrm{s}\psi_{\mathrm{d}} \end{bmatrix} \begin{bmatrix} {}^N\ddot{x}_{\mathrm{d}} \\ {}^N\ddot{y}_{\mathrm{d}} \end{bmatrix}, \tag{25}$$

and $\dot{\phi}_{\mathrm{d}}$ and $\dot{\theta}_{\mathrm{d}}$ are obtained by using equations (22) and (25) as

$$\begin{aligned} \dot{\phi}_{\mathrm{d}} &= -\frac{m}{u_{\mathrm{th}}} \left(k_a \dot{e}_y + d_a \ddot{e}_y + i_a e_y \right), \\ \dot{\theta}_{\mathrm{d}} &= \frac{m}{u_{\mathrm{th}}} \left(k_a \dot{e}_x + d_a \ddot{e}_x + i_a e_x \right), \end{aligned} \tag{26}$$

where ψ_d and $\dot{\psi}_{\mathrm{d}}$ are the required constant value in accordance with the path-tracking mission, and they are simply assumed as zeros without loss of generality. The control of ψ is distinct from the control of ϕ and θ since ψ is not related to the translational motion. For the translational motion along the X and Y axes, it is requisite for controlling ϕ and θ from equations (25) and (26).

2.4. Calculation of α and β for Generating $\boldsymbol{\tau}$. Figure 3 describes a control scheme for the SUAV. The CG variation has no effect on u_{th} with respect to $\mathbf{T}$. The combination of u_{th} and the weight of the moving part, however, generates $\boldsymbol{\tau}$ for controlling attitude. In equation (24), $\boldsymbol{\tau}$ for the attitude control in the body-fixed coordinate generated from the position of the moving part in equation (4), u_{th}, and the weight of the moving part is expressed as

$$\boldsymbol{\tau} = \mathbf{r}_{\mathrm{p}} \times \left(m_{\mathrm{p}} C_N^B \mathbf{g} - \mathbf{T} \right), \tag{27}$$

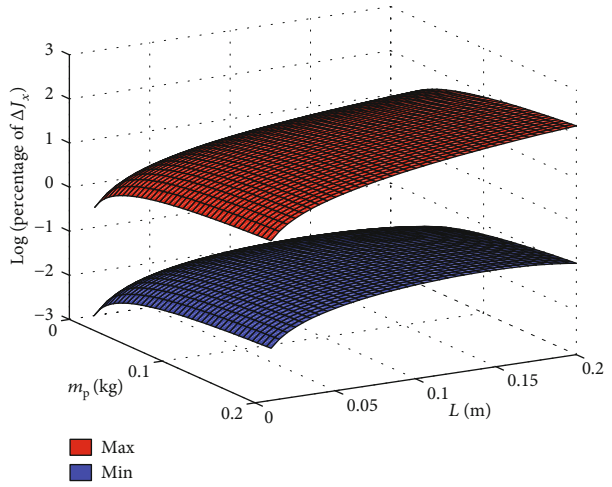

FIGURE 4: ΔJ_x w.r.t. m_p and L variation.

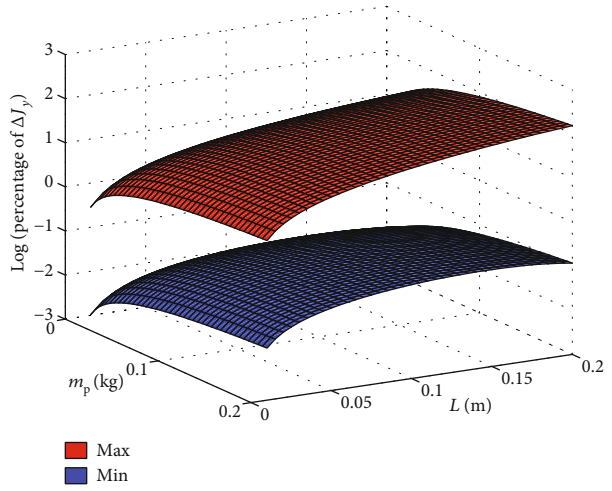

FIGURE 5: ΔJ_y w.r.t. m_p and L variation.

where $\mathbf{r} \in \mathscr{R}^3$ is the position and $C_N^B = (C_B^N)^T$. From equation (27), the desired position of the moving part in the body-fixed coordinate can be expressed as

$$\mathbf{r}_{p,d} = \left[\mathbf{T} - m_p C_N^B \mathbf{g}\right]_\times^{-1} \boldsymbol{\tau}, \tag{28}$$

where $[\boldsymbol{\eta}]_\times$ denotes a skew-symmetric matrix for an arbitrary vector $\boldsymbol{\eta} = [\eta_1, \eta_2, \eta_3]^T$ as follows:

$$[\boldsymbol{\eta}]_\times = \begin{bmatrix} 0 & -\eta_3 & \eta_2 \\ \eta_3 & 0 & -\eta_1 \\ -\eta_2 & \eta_1 & 0 \end{bmatrix}. \tag{29}$$

From equations (4) and (28), α_d and β_d to follow the desired path are obtained as

$$\begin{aligned} \beta_d &= \operatorname{atan2}\left(r_{p,d,y}, r_{p,d,x}\right), \\ \alpha_d &= s^{-1}\left(\frac{r_{p,d,x}}{Lc\beta_d}\right) \end{aligned} \tag{30}$$

Note that the double-variable-based arctangent function is used for calculating β_d. Around the hovering or only vertical movement positions, $[\mathbf{T} - m_p C_N^B \mathbf{g}]_\times$ in equation (28) would be the row rank matrix, and α_d cannot be determined from $r_{p,d,z}$. To resolve this problem and obtain the stable solution with respect to α_d, α_d is calculated from $r_{p,d,x}$.

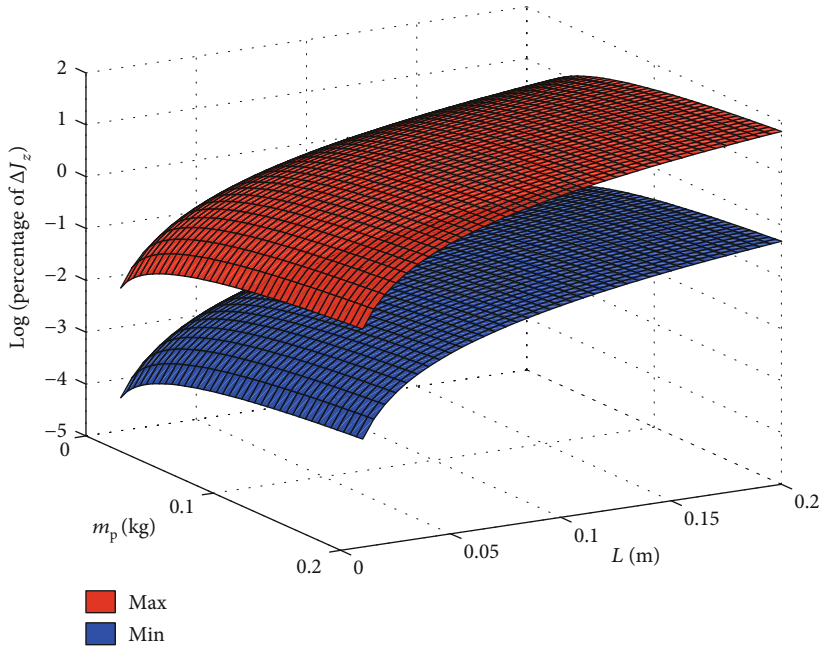

Figure 6: ΔJ_z w.r.t. m_p and L variation.

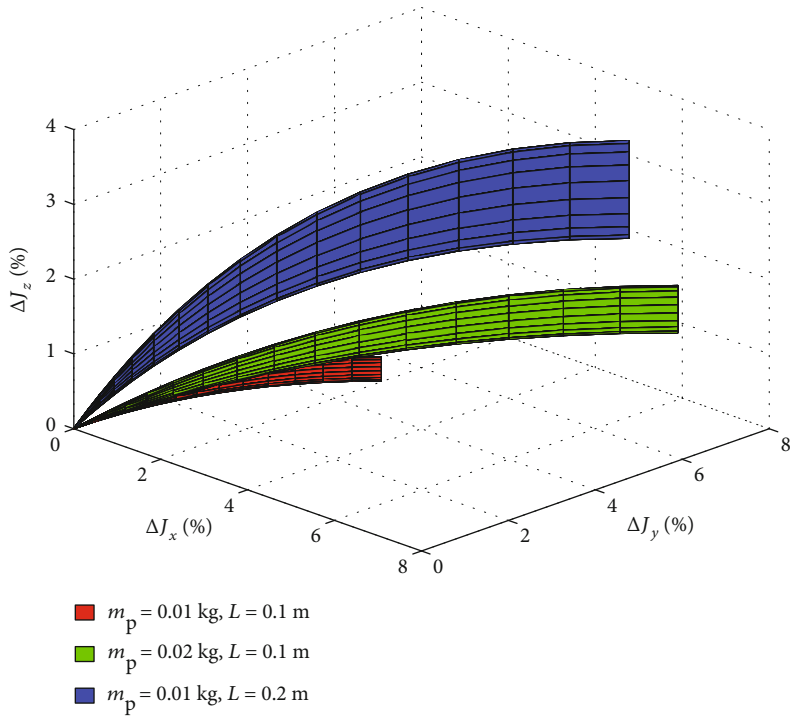

Figure 7: ΔJ_k w.r.t. m_p and L variation.

3. Numerical Simulation

The established path is composed of the following four flight conditions: ascent, horizontal movement, descent, and hovering as listed in Table 1. The trajectory is mainly designed to verify whether the proposed method works properly under the two following conditions. First, the moving part operates properly in the lateral motion to maneuver the SUAV in the combination of four cardinal directions. Second, the yaw angle does not change largely when increasing the altitude at the same time as the operation of the moving parts. If the SUAV proposed met both conditions, the feasibility of the CG-driven UAV system could be confirmed.

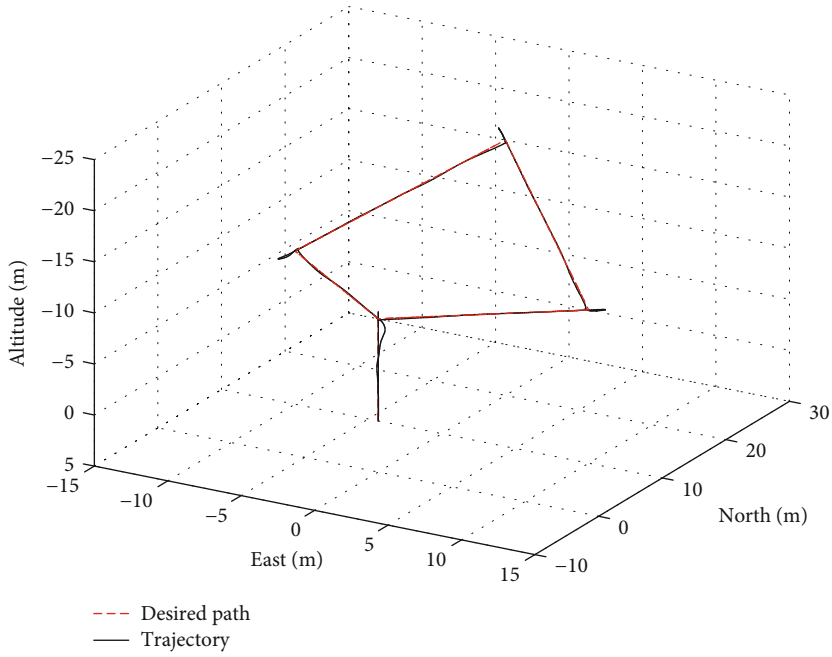

Figure 8: 3D trajectory of the SUAV.

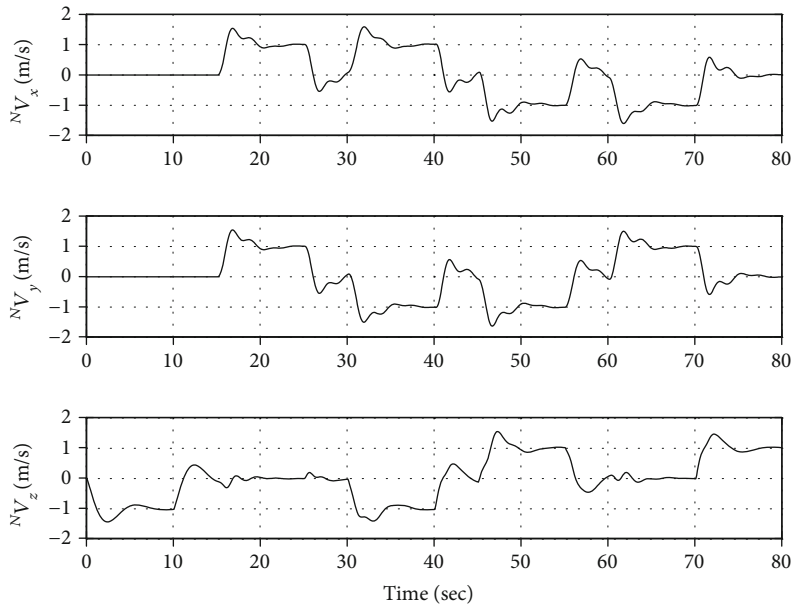

Figure 9: Time history of velocities.

The simulation conditions are shown in Table 2. The stability of the closed-loop system suggested is stable because all poles are located on the left hand plane as follows: -0.0521 and $-1.5118 \pm 1.1839i$ in altitude, $(-0.0028, -1.7353) \times 10^3$ in roll (ϕ) and pitch (θ), and $(-0.0028, -1.7569) \times 10^3$ in yaw (ψ), respectively. Figures 4–6 represent the maximum and the minimum changes of ΔJ_x, ΔJ_y, and ΔJ_z with respect to m_p and L variations, respectively. *Note that the logarithmic scale is used to facilitate classification between the maximum and the minimum changes of MOI elements.* As shown, ΔJ_x, ΔJ_y, and ΔJ_z vary up to about 153.6%, 153.6%, and 63.8% at most and 0.16%, 0.16%, and 0.48% at least, respectively. Figure 7 represents the variations of the MOI elements with respect to m_p and L variations as an example. Figures 4–7 are obtained by using equation (7) at $|\alpha| \leq 90^\circ$ and $\forall \beta$. As shown in Figure 7, the mass change of the moving part affects the variation of J_x and J_y mainly, and all inertia properties are affected by the variation of the rod length of the moving part.

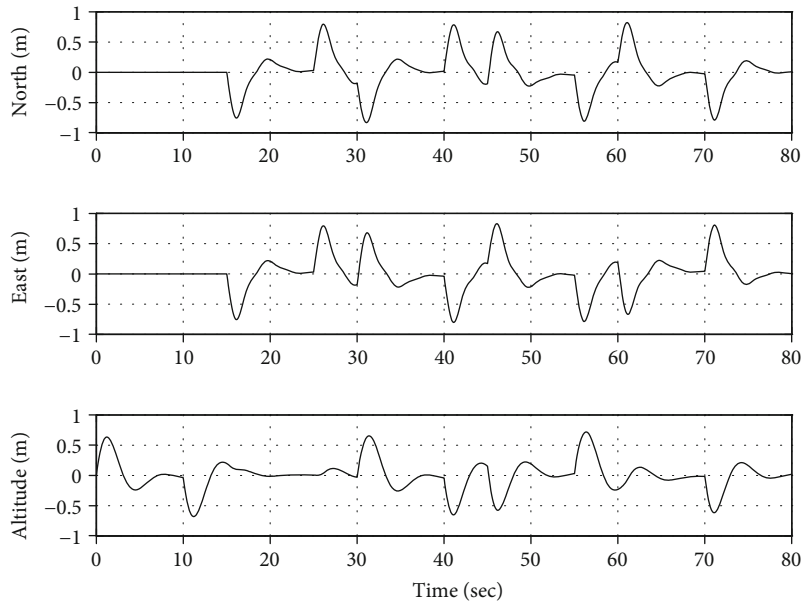

Figure 10: Time history of position error.

Table 3: Error between desired path and trajectory.

Parameter	North	East	Altitude
MAE (m)	0.8353	0.8292	0.7170
RMSE (m)	0.2926	0.2850	0.2517

Since both the mass and the rod length of the moving part are related to the amount of the generating torque for attitude control, it is necessary to increase the mass of the moving part for a large amount of generating torque and a low variation of the inertia properties. In other words, the MOI elements are affected by both m_p and L, and L is the more dominant factor to influence the change of the MOI elements.

Figures 8 and 9 represent the three-dimensional (3D) trajectory of the SUAV captured with the desired path and the velocities of the SUAV, respectively. It is shown that the SUAV with the designed control law follows the designated path listed in Table 1. Figure 10 and Table 3 show that the trajectory errors in all directions are less than 0.84 m. One reason for such a result is that the SUAV system proposed is the underactuated system. The SUAV only generates a thrust force that has an upward direction with respect to the body-fixed frame. In the case of lateral motion, it is necessary to combine the attitude and the thrust. Although the control law is derived by using this relationship between the attitude and the thrust, the decelerating force is not enough to come to a halt at each waypoint in time. This path-tracking error could be improved by applying a type of nonlinear adaptive controller, but this is not the scope of this work at this time. The maximum absolute error (MAE) and the root mean square error (RMSE) in Table 3 are calculated as

$$\text{MAE} = \max |\mathbf{e}_k|,$$
$$\text{RMSE} = \sqrt{\frac{\mathbf{e}_k^T \mathbf{e}_k}{n}}, \tag{31}$$

where $k = x,y$, and z, and n is the total number of the data.

The time histories of Euler angles, which are the attitude of the SUAV, and the corresponding control inputs to achieve both the desired position and attitude of the SUAV are described in Figures 11 and 12. Note that ψ is not equal to zero in spite of u_ψ being equal to zero because the torque of ${}^BZ$ axis for rotating ψ is generated from the weight of the moving part according to the attitude of the SUAV. Figure 13 represents the time history of α and β of the moving part for the SUAV control, and the corresponding CG variation is shown in Figure 14. The CG variations do not exceed 1 centimeter over time, and this surely indicates that inertia variation is small enough to ignore the effect of parametric uncertainty. Figure 15 shows the position of the moving part for the path-tracking mission according to the phases listed in Table 1. During phases A and B, which are the ascent and hovering modes, the moving part does not need to behave since no attitude changes are required. In the case of phases C, E, G, and I, the moving part is operated to follow the desired path. In the case of phases D, F, H, and J, the moving part is operated for braking purposes for about 0.1 sec and then for keeping all attitude equals to zero.

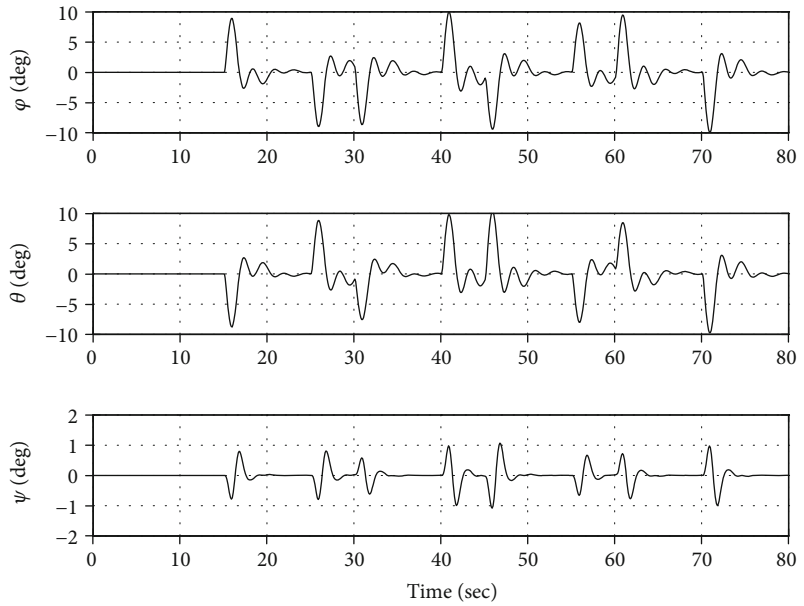

Figure 11: Time history of Euler angles.

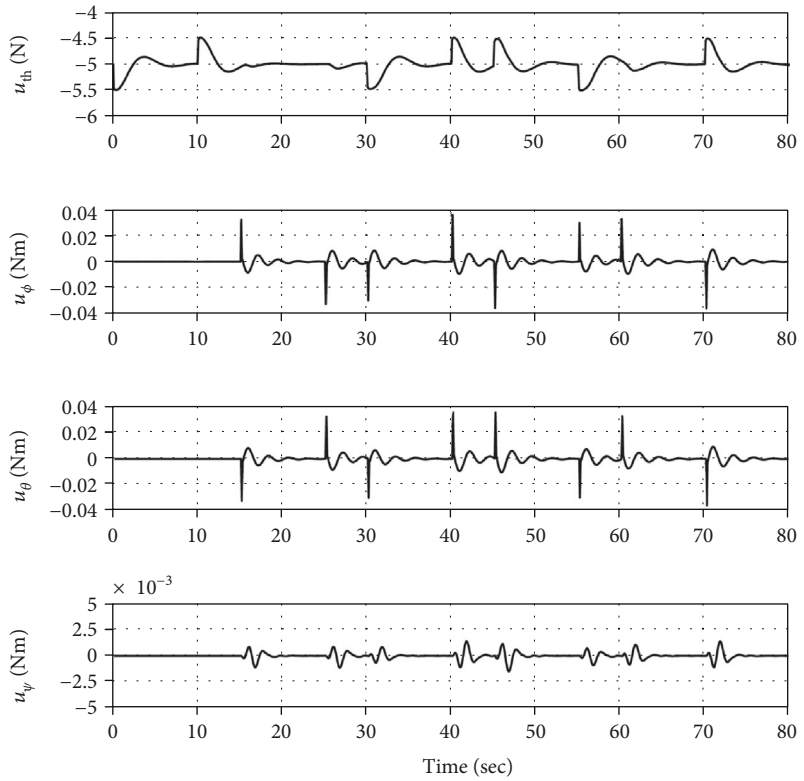

Figure 12: Time history of control inputs.

4. Conclusion

This paper presents a conceptual design of a spherical unmanned aerial vehicle (SUAV) with a center-of-gravity (CG) variation-based path-tracking control law, and it works with the following three steps: (1) the control inputs are calculated from the path-tracking controller; (2) the required position of the moving part is calculated from the control inputs; and (3) the rotating angles of the moving part are calculated from the required position of the moving part. The

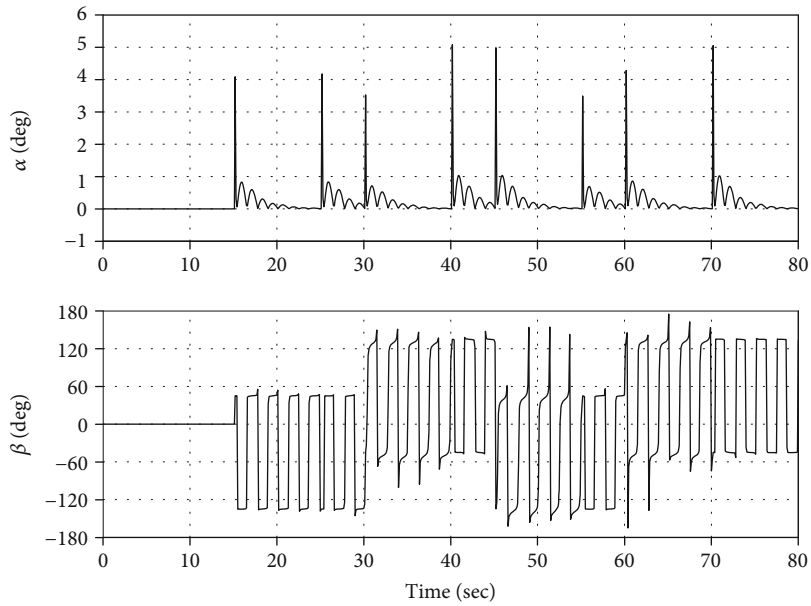

Figure 13: Time history of α and β.

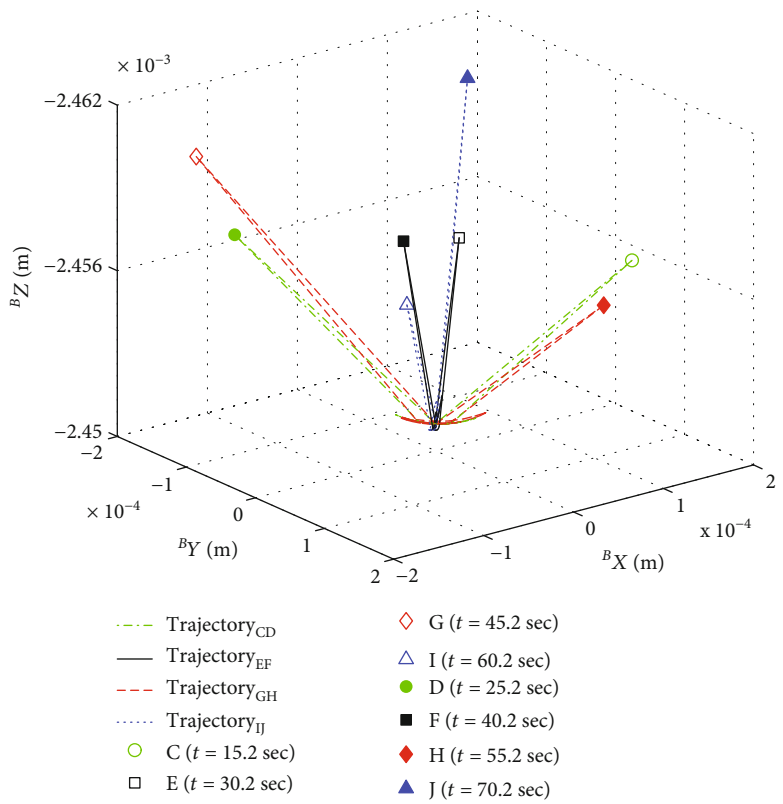

Figure 14: 3D position of the CG for the SUAV.

position of the moving part, which varies the CG, is controlled by a stepping motor and a DC motor providing two degrees-of-freedom such as elevation and azimuth angles. The control torques for attitude control with respect to roll and pitch motions can be generated from the combination of the position, the mass of the moving part, and the thrust force from a rotor. The changed position of the moving part results in the variation of MOI, and this variation has an effect on the performance of the suggested method. The variation of MOI analysis is performed under angular ranges of

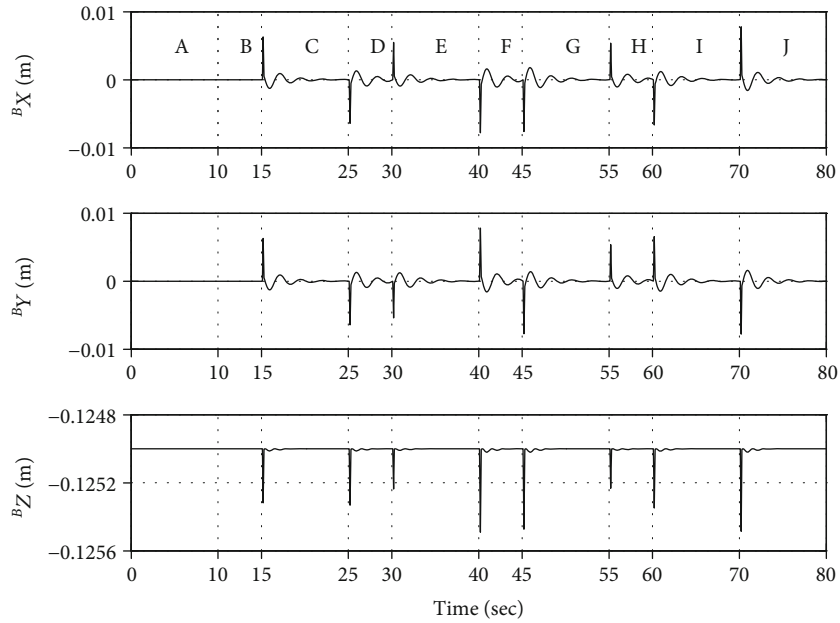

Figure 15: Position of the moving part w.r.t. phases.

elevation and azimuth. Based on the analysis, the rod length and the moving part mass are determined to avoid the effect of the MOI variation on the control performance. Numerical simulation results demonstrate the feasibility of operations of the SUAV proposed with the path-tracking control law.

Data Availability

The [simulation parameters] data used to support the findings of this study are included within the article.

Conflicts of Interest

The authors declare that there is no conflict of interests regarding the publication of this paper.

Acknowledgments

This research was supported by the faculty start-up fund at the University of Cincinnati.

References

[1] C. R. Ashokkumar, G. W. P. York, and S. Gruber, "Trustable UAV for higher level control architectures," *Aerospace Science and Technology*, vol. 68, pp. 204–213, 2017.

[2] M. S. Francis, "Unmanned air systems: challenge and opportunity," *Journal of Aircraft*, vol. 49, no. 6, pp. 1652–1665, 2012.

[3] W. W. Greenwood, J. P. Lynch, and D. Zekkos, "Applications of uavs in civil infrastructure," *Journal of Infrastructure Systems*, vol. 25, pp. 1–21, 2019.

[4] J. Rubio-Hervas, A. Gupta, and Y.-S. Ong, "Data-driven risk assessment and multicriteria optimization of uav operations," *Aerospace Science and Technology*, vol. 77, pp. 510–523, 2018.

[5] B. Loh and J. D. Jacob, "Modeling and attitude control analysis of a spherical vtol aerial vehicle," in *51st AIAA Aerospace Sciences Meeting*, pp. 1–15, Dallas, TX, USA, 2013.

[6] K. Malandrakis, R. Dixon, A. Savvaris, and A. Tsourdos, "Design and development of a novel spherical uav," *IFAC-PapersOnLine*, vol. 49, no. 17, pp. 320–325, 2016.

[7] F. Sato, *Digital Content Expo*, Technical Research and Development Institute at Japan's Ministry of Defense, 2011, https://theaviationist.com/tag/digital-content-expo/.

[8] G. B. Kim, N. S. Goo, K. J. Yoon, H. C. Park, and Y. H. Yu, "Design, fabrication, and performance test of a rotary-wing micro aerial vehicle," *Journal of Aircraft*, vol. 43, no. 2, pp. 564–566, 2006.

[9] C. Bermes, K. Sartori, D. Schafroth, S. Bouabdallah, and R. Siegwart, "Control of a coaxial helicopter with center of gravity steering," in *Proceedings of the International Conference on Simulation, Modeling and Programming for Autonomous Robots*, pp. 492–500, Venice, Italy, 2008.

[10] S. Bouabdallah, R. Siegwart, and G. Caprari, "Design and control of an indoor coaxial helicopter," in *2006 IEEE/RSJ International Conference on Intelligent Robots and Systems*, pp. 2930–2935, Beijing, China, 2006.

[11] F. Z. Seisan, *Modeling and control of a co-axial helicopter, [M.S. thesis]*, Electrical and Computer Engineering Department, Toronto University, 2012.

[12] Y. Choi, S. Yang, J. Yang, B. Kim, and S. Lee, "A study on performance of path tracking controller using changes in center of gravity of spherical uav," in *2015 KSAA Fall Conference*, pp. 50–54, Incheon, Republic of Korea, 2015.

[13] E. Altuğ, J. P. Ostrowski, and C. J. Taylor, "Control of a quadrotor helicopter usingˇ dual camera visual feedback," *International Journal of Robotics Research*, vol. 24, no. 5, pp. 329–341, 2005.

[14] T. Sangyam, P. Laohapiengsk, W. Chongcharoen, and I. Nikhamhang, "Path tracking of uav using self-tuning pid controller based on fuzzy logic," in *2010 IEEE/SICE Annual Conference*, pp. 1265–1269, Taipei, Taiwan, 2010.

[15] A. M. Kamal, A. M. Bayoumy, and A. M. Elshabka, "Modeling and flight simulation of unmanned aerial vehicle enhanced with fine tuning," *Aerospace Science and Technology*, vol. 51, pp. 106–117, 2016.

[16] H. Schaub and J. L. Junkins, "Analytical Mechanics of Space Systems," in *AIAA Education Series, AIAA*, pp. 129–131, Reston, VA, 2003.

[17] A. Nagaty, S. Saeedi, C. Thibault, M. Seto, and H. Li, "Control and navigation framework for quadrotor helicopters," *Journal of Intelligent and Robotic Systems*, vol. 70, no. 1-4, pp. 1–12, 2013.